Validation of Computational Ship Air Wakes for a Naval Research Vessel

Murray R. Snyder[1,2]
George Washington University, Washington, DC 20052
United States Naval Academy, Annapolis, MD 21402

Anil Kumar[3] and Pinhas Ben-Tzvi[4]
George Washington University, Washington, DC 20052

Hyung Suk Kang[5]
Johns Hopkins University Applied Physics Laboratory, Laurel, MD 20723

This paper provides current results of a multi-year research project that involves the systematic investigation of ship air wakes using an instrumented United States Naval Academy (USNA) YP (Patrol Craft, Training). The objective is to validate and improve Computational Fluid Dynamics (CFD) tools that will be useful in determining ship air wake impact on naval rotary wing vehicles. This project is funded by the Office of Naval Research and includes extensive coordination with Naval Air Systems Command. Currently, ship launch and recovery wind limits and envelopes for helicopters are primarily determined through at-sea *in situ* flight testing that is expensive and frequently difficult to schedule and complete. The time consuming and potentially risky flight testing is required, in part, because computational tools are not mature enough to adequately predict air flow and wake data in the lee of a ship with a complex superstructure. The top-side configuration of USNA YPs is similar to that of a destroyer or cruiser, and their size (length of 108 ft and above waterline height of 24 ft) allows for collection of air wake data with a Reynolds number that is the same order of magnitude as that of modern naval warships, an important consideration in aerodynamic modeling. A dedicated YP has been modified to add a flight deck and hangar-like structure to produce an air wake similar to that from a modern destroyer. Three-axis acoustic anemometers have been installed at various locations, including a large vertical array on the ship's bow to measure atmospheric boundary layers. Repeated testing on the modified YP is being conducted in the Chesapeake Bay, which allows for the collection of data over a wide range of wind conditions. Additionally, a 4% scale model of the modified YP has been constructed and tested in the USNA recirculating wind tunnel. Comparison of YP *in situ* data with similar data from wind tunnel testing and CFD simulations shows reasonable agreement for a headwind condition and for relative winds 15° and 30° off the starboard bow. Analysis also indicates that CFD simulations require modeling the velocity profile in the atmospheric boundary layer to improve simulation accuracy. Finally, off-ship turbulence data collected using an instrumented 4.5 ft rotor diameter radio controlled helicopter show that the detected off-ship air wake is present where predicted by CFD simulations.

---

[1] Research Professor, George Washington University, Mechanical and Aerospace Engineering Department, 725 23rd Street NW, AIAA Member.
[2] Research Professor, US Naval Academy, Aerospace Engineering Department, 590 Holloway Road.
[3] Graduate Student, Mechanical and Aerospace Engineering Department, 801 22nd Street NW.
[4] Assistant Professor, Mechanical and Aerospace Engineering Department, 801 22nd Street NW.
[5] Senior Professional Staff, 11100 Johns Hopkins Road.

Nomenclature

A_ω = Air Wake Data
CAD = Computer Aided Design
CFD = Computational Fluid Dynamics
IMU = Inertial Measurement Unit
LHA = General Purpose Amphibious Assault Ship
MILES = Monotone Integrated Large Eddy Simulation
USNA = United States Naval Academy
YP = Patrol Craft, Training
β = relative wind angle on horizontal plane
H = height of hangar structure
x = distance aft of hangar
y = distance port or starboard of ship centerline, positive to starboard
z = distance above flight deck
u_{fit} = least-square curve fitted boundary layer velocity
U_R = bow reference anemometer velocity
U_{YP} = YP velocity

I. Introduction

LAUNCH and recovery of rotary wing aircraft from naval vessels can be very challenging and potentially hazardous. Ship motion combined with the turbulence that is created as the wind flows over the ship's superstructure can result in rapidly changing flow conditions for rotary wing aircraft. Additionally, dynamic interface effects between the vessel air wake and the rotor wake are also problematic.

To ensure aircraft and vessel safety, launch and recovery envelopes are prescribed for specific aircraft types on different ship classes (Fig. 1).[1] Permissible launch and recovery envelopes are often restrictive because of limited flight envelope expansion. Flight testing required to expand the envelopes is frequently difficult to schedule, expensive and potentially hazardous. Currently, the launch and recovery wind limits and air operation envelopes are primarily determined via the subjective analysis of test pilots (e.g. excessive flight control inputs are required to safely land on the flight deck), using a time consuming and potentially risky iterative flight test build-up approach. The time and risk of flight testing could be reduced through the complementary use of computational tools to predict test conditions and extrapolate test results, thereby reducing the number of actual flight test points required. However, current computational methods are insufficiently validated for ships with a complex superstructure, such as a destroyer or cruiser.[2-9] Validated computational air wake predictions can also be used for ship design and operational safety analysis.
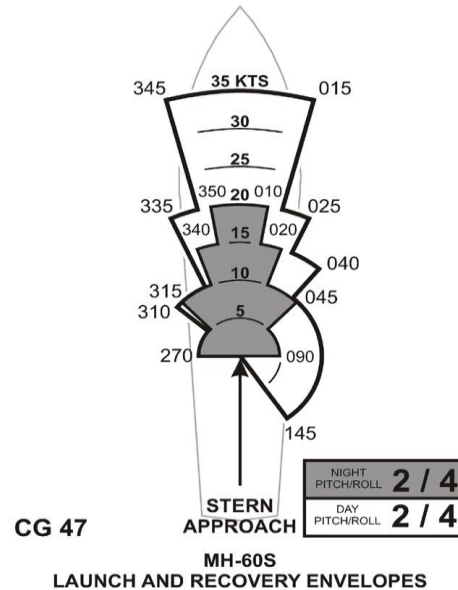
Figure 1. Launch and recovery envelopes, showing allowable relative wind over deck, for MH-60S helicopters on USS Ticonderoga (CG 47) class cruiser (Ref. 1).

American Institute of Aeronautics and Astronautics

This paper presents an update of a multi-year project to develop and validate Computational Fluid Dynamics (CFD) tools to reduce the amount of at-sea *in situ* flight testing required and make rotary wing launch and recovery envelope expansion safer, more efficient, and affordable. The authors do not envision these CFD tools as replacing the need for flight testing and the associated human subjective analysis associated with flight testing. Rather, we hope to develop validated CFD tools that will allow a reduction in the amount of flight testing required and to focus the flight testing that is performed on the limits of the launch and recovery envelopes where pilot subjective analysis is particularly important.

II.   Project Description

The Ship Air Wake Project leverages unique resources available at the United States Naval Academy (USNA) that allow for a systematic analysis of ship air wakes.

A.   *In Situ* Measurement of Ship Air Wake

USNA operates a fleet of YP (Patrol Craft, Training) vessels for midshipman training. The USNA YPs (Fig. 2) are relatively large vessels (length of 108 ft (32.9 m) and an above waterline height of 24 ft (7.3m)) with a superstructure and deck configuration that resembles that of a modern destroyer or a cruiser. The size of the YPs is such that air wake data can be collected with Reynolds numbers in the same order of magnitude as those for modern naval warships, an important consideration in aerodynamic modeling. (Reynolds number is the ratio of inertia forces to viscous forces.) As shown in Fig. 3, YP676 has been modified to add a representative flight deck and hangar-like structure that model those on modern US Navy ships.

Ultrasonic anemometers have been installed to allow for direct measurement of relative wind velocities over the flight deck (Fig. 4). The anemometers are the Applied Technology Inc. "A" style three-velocity component model with a 5.91 inch path length and a measurement accuracy of ± 1.18 inch/s. The anemometers are connected to a synchronizer that allows up to 8 different anemometers to be sampled simultaneously at up to 20 Hz. As of the submission of this paper, over 50 underway test periods in the Chesapeake Bay have been completed. Air wake velocity data have been collected at 162 points between 16.5 and 83 inches above the flight deck for winds up to 17 knots (nautical mile/hr) for three different incoming flow conditions, i.e., a head wind condition and winds 15° and 30º off the starboard bow.

Figure 2. USNA YP676.

Figure 3. Detail of YP676 flight deck and hangar-like structure.

Figure 4.   Ultrasonic anemometers installed on YP676 flight deck.

B. Wind Tunnel Measurements

Wind tunnel tests of a 4% scale model of the YP were completed in USNA's recirculating wind tunnel (with a test section of 42-inch in height × 60-inch in width × 120-inch in length) in November 2010 and October 2012. Figure 5 shows the YP model in the wind tunnel with the 18 hole Omniprobe that is used to collect three-dimensional velocity data over the flight deck and adjacent areas. (Figure 5 shows the model that was tested in November 2010. The testing performed in October 2012 included passive flow control wedges that will be discussed in Section V.)

The wind tunnel tests were conducted at a test section free stream velocity of 300 ft/s to match the Reynolds number of the YP experiencing a 7 knot relative wind. (Reynolds numbers are matched for appropriate ship length scales such as ship length or hanger height.) Velocity data were collected at 1855 points above and around the model flight deck for a fixed incoming velocity.
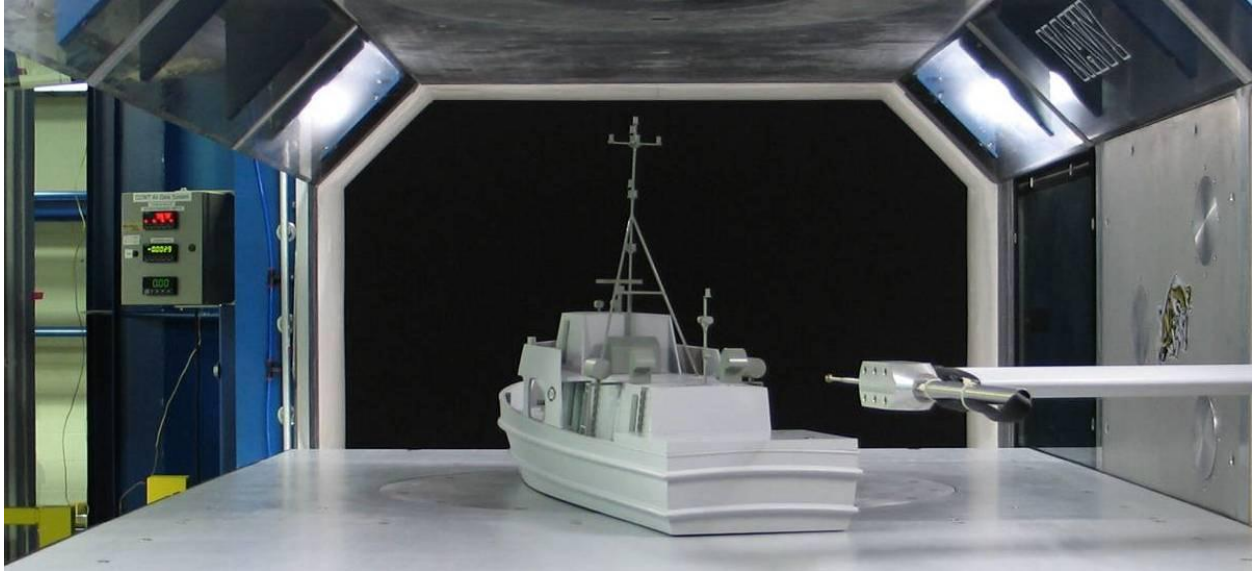

Figure 5. 4% scale YP model in USNA wind tunnel.

C. Computational Fluid Dynamics Simulations

Numerical simulations have been performed by USNA midshipmen using Cobalt,[10] a commercial parallel processing CFD code which uses an unstructured tetrahedral grid system. As shown in Fig. 6, the unstructured grid allows for finer resolution near boundaries and in other regions where more complicated flow structures are expected.

The tetrahedral grids are divided into partitions to allow parallel processing on advanced computer clusters. Such partitioning speeds up the solution generation by allowing an individual processor to solve the flow field in a limited number of tetrahedral.

Midshipmen have performed CFD analysis for both 7 and 20 knots of relative wind. CFD simulations, using an unstructured grid system of approximately 15.5 million tetrahedral, have been completed for a head wind and for winds from the starboard bow (or relative wind angle β) of 15°, 30°, 45°, 60°, 75° and 90°. These analyses used a Monotone Integrated Large Eddy Simulation (MILES), which is a laminar, time accurate flow model.[11] In a study involving an LHA Class US Navy ship, the MILES approach has been shown to correctly predict dominant frequencies in the measured flow field during *in situ* testing with four anemometers installed on the flight deck and in concurrent 1/120th scale model wind tunnel testing.[12]
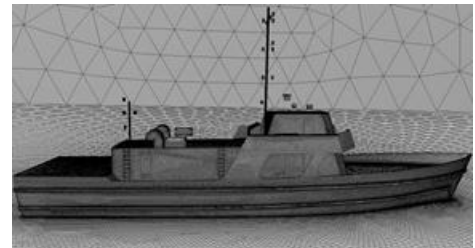
Figure 6. Unstructured surface grid.

III. Prior Results

As mentioned above, over 50 underway test periods in the Chesapeake Bay have been completed. These underway test periods last typically 6 to 8 hours and include 5 or 6 data collection periods of 20-30 minutes at a specified incoming relative wind condition. Weather conditions can vary widely with typical sea states of 3 or less (with a maximum observed wave height of approximately 4 feet (1.2 m) during storm conditions). Using up to 8 anemometers simultaneously, *in situ* data have been collected for a head wind, and winds nominally 15° and 30° off the starboard bow. Data have been collected from the bow reference anemometer, see Fig. 7, and for anemometers mounted at various heights from 16.5 to 83 inches above the flight deck as shown in Fig. 4. During underway data collection periods, real time data output from the reference anemometer (third from bottom of Fig. 7) is continuously monitored to ensure desired relative wind is approximately maintained and that data quality is satisfactory. This information is also displayed on the YP's bridge such that the ship's helmsman can take corrective action to adjust ship heading. Furthermore, only data that are collected within ± 5° of the desired β is used for comparison with wind tunnel and CFD results.

In prior updates to this project,[13-24] we noted the following results:

Figure 7. Bow anemometer array. Reference anemometer is third from bottom.

1. Initial CFD analysis done in the summer of 2009 on an unmodified YP model was useful in determination of sensor placement on the modified YP676.

2. As one would expect, turbulent kinetic energy is significantly greater in the superstructure wake than in the free stream flow observed by the bow reference anemometer.

3. Minor ship pitch and roll motions, as measured by an installed inertial measurement unit (IMU), have negligible impact on the mean velocity fields in the air wake.

4. Spatial velocity correlations show, as predicted by CFD analysis, a distinctive shear layer present aft of the hangar-like superstructure with the largest scale turbulent eddy which is approximately the same size as the height of the superstructure. A similar shear layer with associated recirculation zone has also been observed in flow visualizations with fog generators.

5. CFD simulations and *in situ* measurements at the bow reference anemometer location show good agreement for the induced vertical velocity component arising from ship interference effects.

6. Over numerous underway test periods, good measurement repeatability has been consistently observed.

7. As shown in Fig. 8 and 9, for β=0° and β=15° respectively, good comparison has been observed between scaled *in situ* and CFD simulation data for numerous locations above the flight deck. (The *in situ* data are scaled to have the same mean velocity magnitude as the CFD simulation at the bow reference anemometer.) The observed comparison in velocity direction, though, is better than in velocity magnitude. Also, similar large scale flow structures are observed in both *in situ* measurements and numerical simulations.

American Institute of Aeronautics and Astronautics

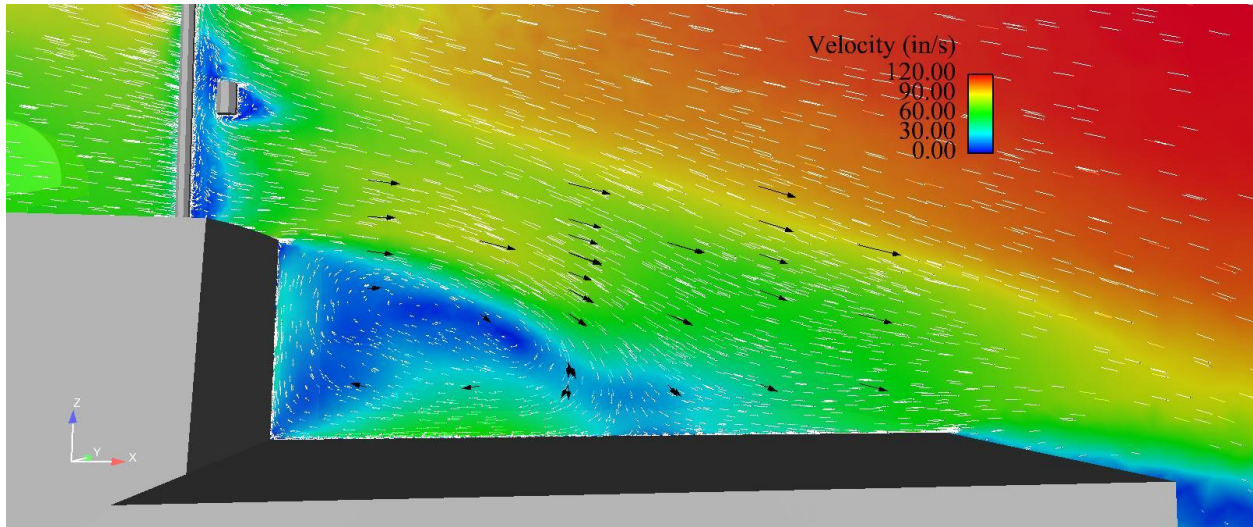**Figure 8. Scaled *in situ* data (black arrows) vs. 7 knot CFD simulations (white arrows and color contours) for headwind (β = 0°) at centerline of the flight deck (7 knots = 141 in/s).**
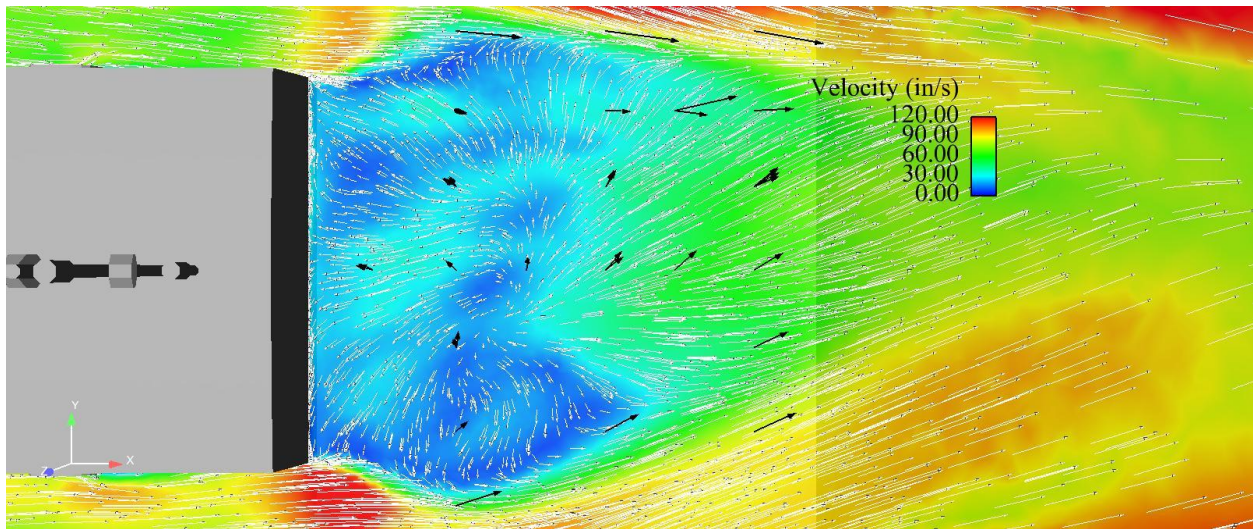

Figure 9. Scaled *in situ* data (black arrows) vs. 7 knot CFD simulations (white arrows and color contours) for relative wind β = 15° for the horizontal plane 17 inches above the flight deck (7 knots = 141 in/s).

8. As shown in the vertical and horizontal planes of Fig. 10 to 15, for β = 0, 15 and 30°, there is reasonable agreement between collected *in situ* and wind tunnel data with CFD flow simulations, with better agreement in velocity direction, with typically less than 15° difference between the three data sets, than in magnitude. (In Fig. 10 to 15 the black arrows represent the scaled *in situ* data, the red arrows represent scaled wind tunnel data and blue arrows represent the CFD data. Locations with two black arrows represent *in situ* data collected on different underway test periods at the same sampling location. U_R represents the flow direction and scaled magnitude in the horizontal plane observed at the bow reference anemometer. H = 1.5 m is the height of the hangar above the flight deck, x represents the distance aft of the hangar, y represents athwartships offset to starboard from the fore to aft centerline of the ship and z represents vertical distance above the flight deck.) As will be discussed below, the likely source of the observed magnitude disparities is that associated CFD simulations and wind tunnel experimentation do not model the atmospheric boundary layer encountered by the full size ship.
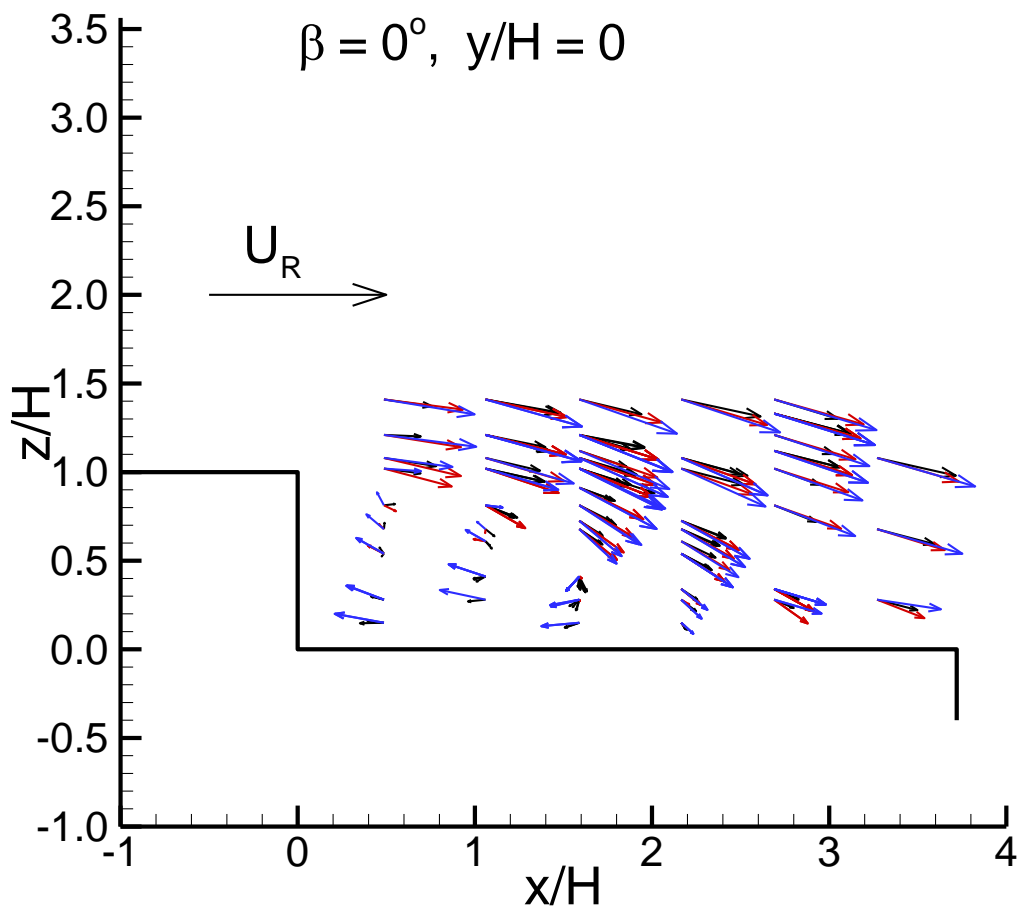
Figure 10. Centerline vertical plane (*y/H* = 0) for a headwind (black arrows are *in situ* data, red arrows are wind tunnel data and blue arrows are CFD data).
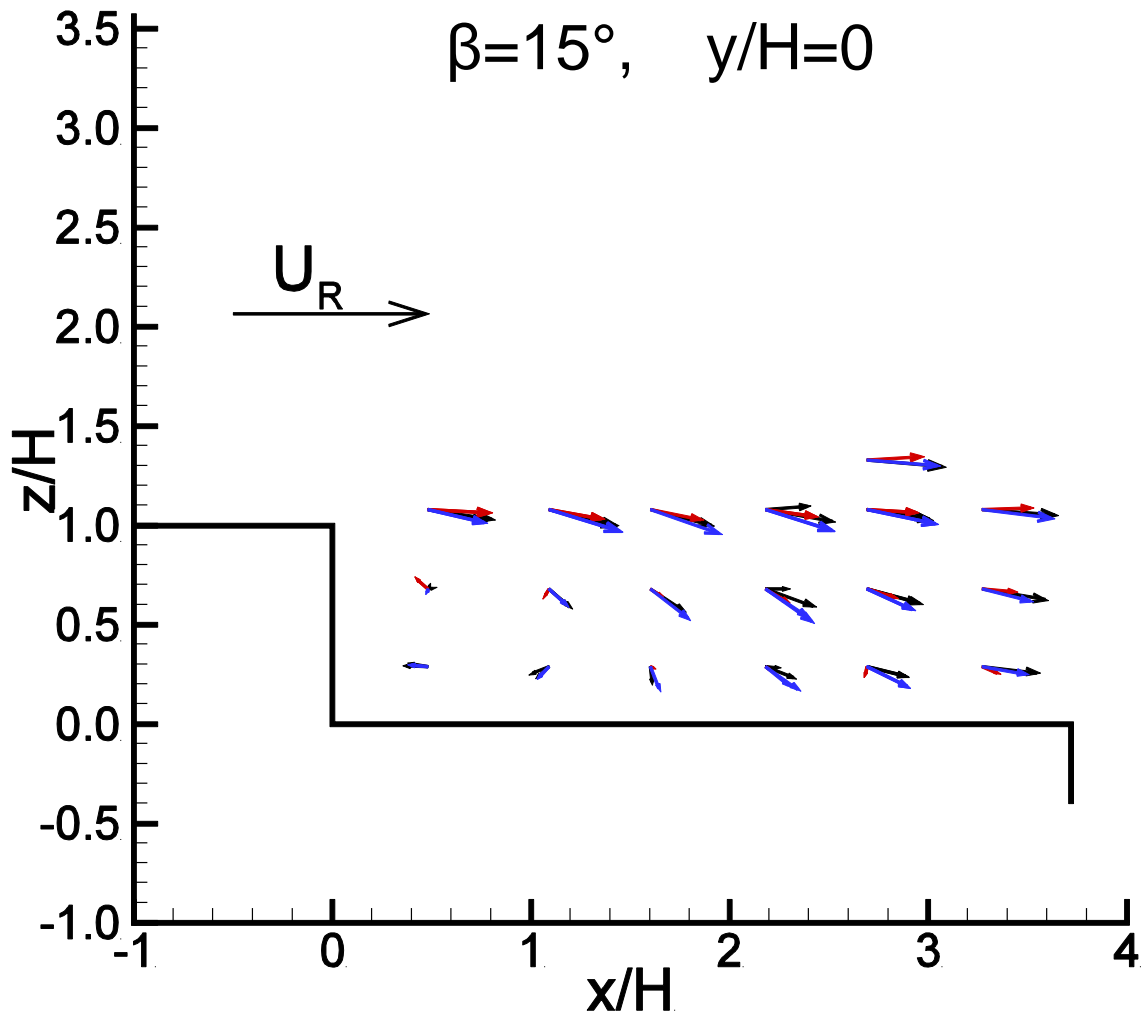
Figure 11. Centerline vertical plane (*y/H* = 0) for relative wind β = 15° (black arrows are *in situ* data, red arrows are wind tunnel data and blue arrows are CFD data).

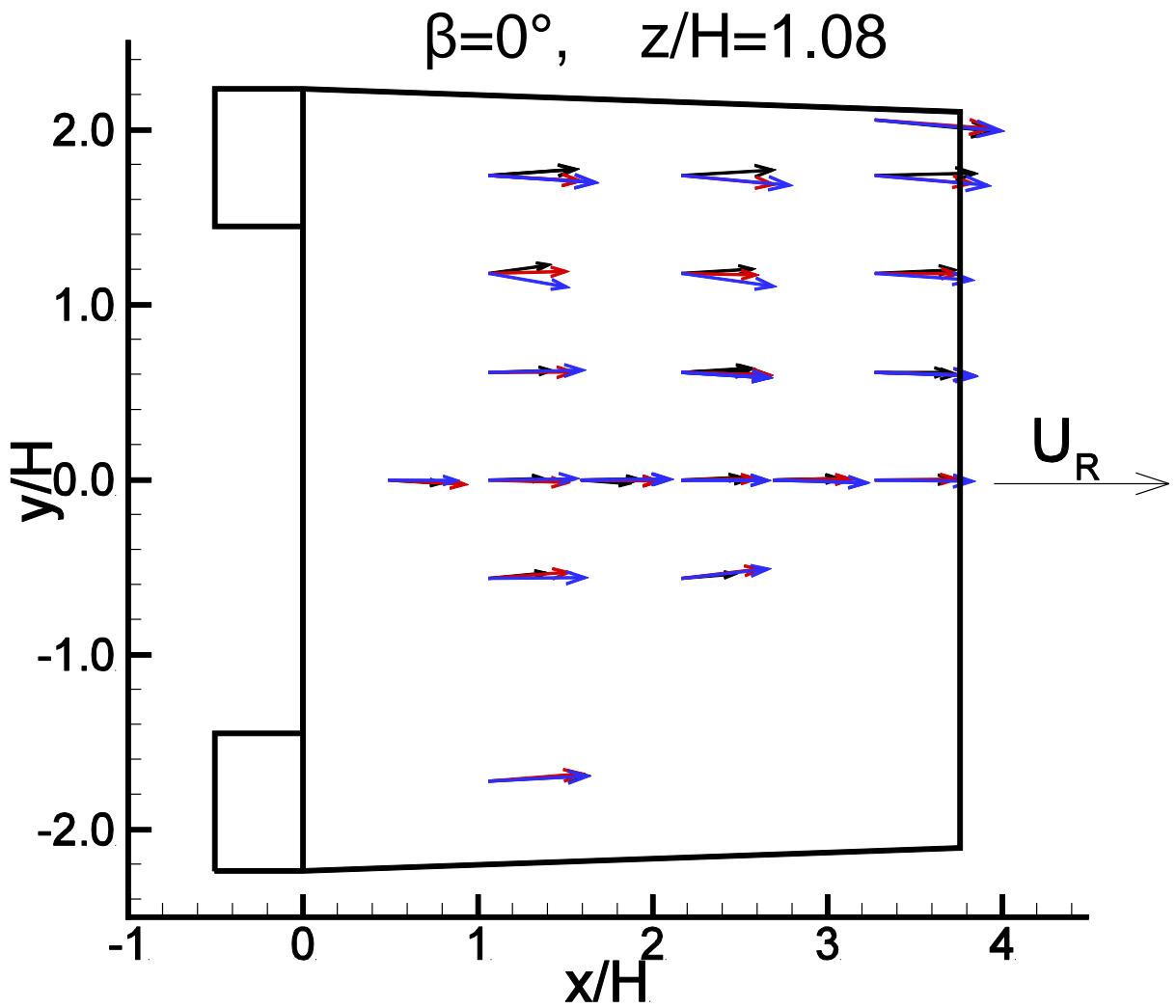American Institute of Aeronautics and Astronautics

Figure 12. Horizontal vertical plane *z/H* **= 1.08 (63.7 inches) above the flight deck for a headwind (black arrows are** *in situ* **data, red arrows are wind tunnel data and blue arrows are CFD data).**
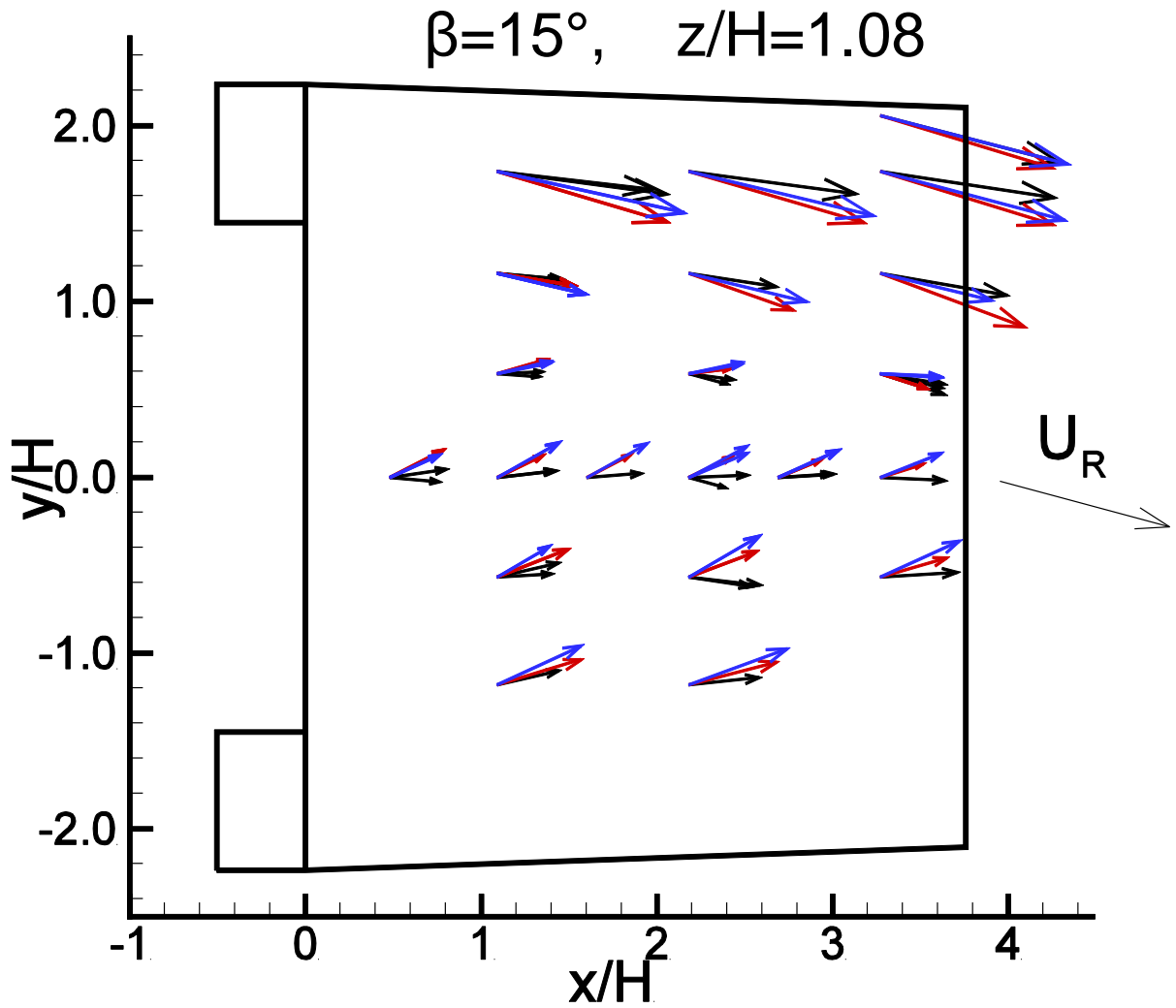
American Institute of Aeronautics and Astronautics

Figure 13. Horizontal vertical plane *z/H* **= 1.08 (63.7 inches) above the flight deck for relative wind β = 15°
(black arrows are** *in situ* **data, red arrows are wind tunnel data and blue arrows are CFD data).**

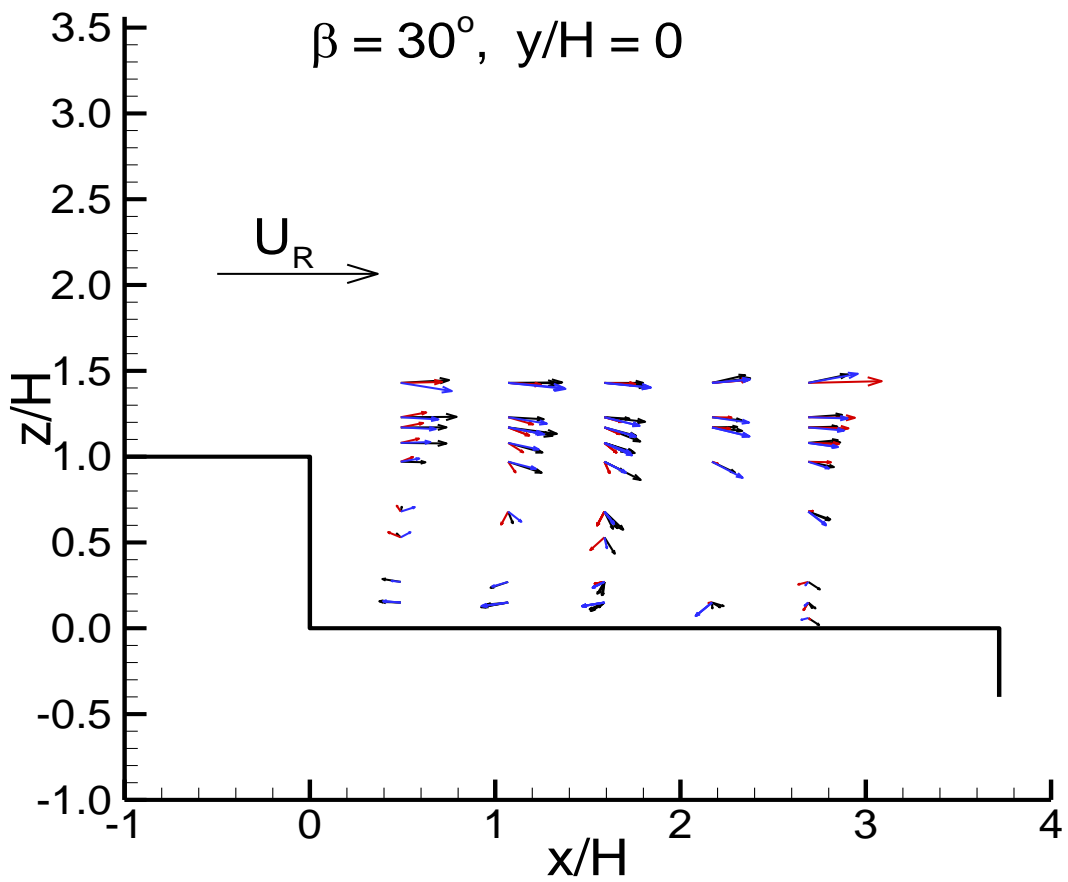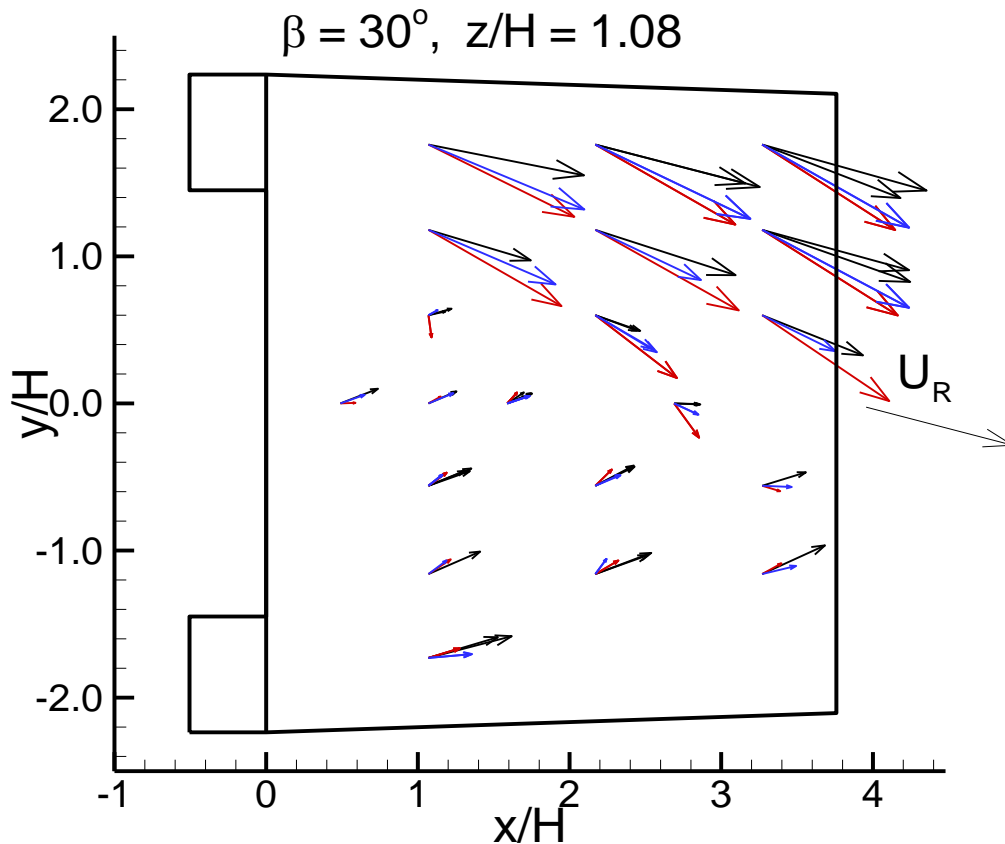American Institute of Aeronautics and Astronautics

Figure 14. Centerline vertical plane (*y/H* = 0) for relative wind β = 30° (black arrows are *in situ*, red arrows are wind tunnel data and blue arrows are CFD data).

American Institute of Aeronautics and Astronautics

Figure 15. Horizontal vertical plane $z/H = 1.08$ **(63.7 inches above the flight deck) for relative wind** $\beta = 30°$ **(black arrows are** *in situ* **data, red arrows are wind tunnel data and blue arrows are CFD).**

9.   There are significant velocity magnitude deviations between the shown CFD simulations, which assume a uniform velocity profile from the ocean surface upward, and with the atmospheric boundary layer measured while underway. In Fig. 16 the fitted power-law velocity profile $(u_{fit} + U_{YP})/U_{Bow}$ (red line) of underway data from July 2011 is compared with that from CFD simulations (blue line). The reference bow anemometer (third anemometer from the bottom of Fig. 7) location is shown with the horizontal green line. Thus, u/U_{Bow} is 1 at the reference bow anemometer height of 5.58 m. The contribution of the YP speed to u/U_{Bow} is 46.4%. The decrease of the CFD velocity near $z = 3$ m is attributed to YP hull shape effects on the incoming flow. Though the velocity magnitude is matched near the bow height, the incoming velocity profile imposed in CFD simulations is uniform ($u/U_{Bow} \sim 1$), which is quite different from the measured mean velocity profile (red line) of the actual atmospheric boundary layer. These results emphasize the importance of including an atmospheric boundary layer profile in CFD simulations.

10.   The highly variable nature of the observed atmospheric boundary layer can be shown through comparison of least square curve fitting ($u_{fit} = a\,(z/b)^m + c$, where z is the distance above the vessel's waterline) of data from different underway periods. Data from July 2011 gave $a = 3.83$, $b = 4.84$, $c = 0.05$ and $m = 0.351$ while that from May 2012 gave $a = 1.06$, $b = 3.24$, $c = 0.00$ and $m = 0.58$.
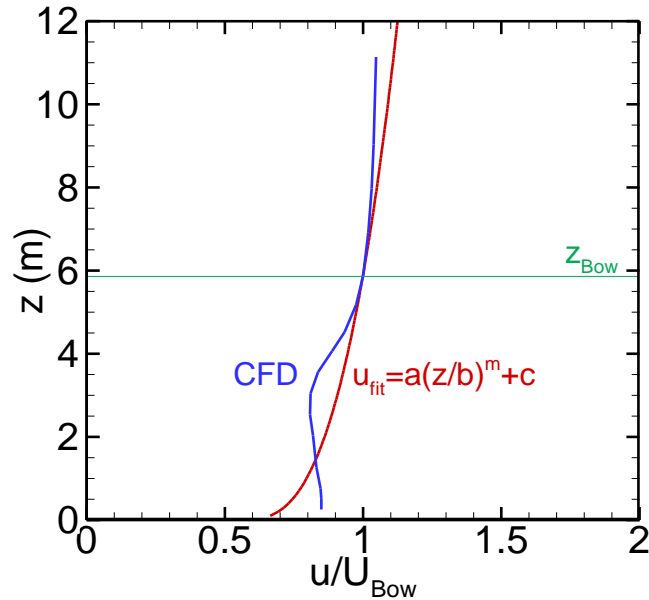
Figure 16: Fitted power law velocity profile (red line) of underway anemometer data vs. CFD velocity profile (blue line). The green line is the height of the bow reference anemometer. (*a, b, c* and *m* are constants determined through least-square curve fitting, *z* is the distance above the vessel's waterline, and *u*$_{fit}$ is the fitted velocity.)

11. During the summer of 2012 Midshipmen interns completed a CFD grid sensitivity study for 17 and 22 million tetrahedral. As shown graphically in Fig. 17, no significant differences were noted between the two simulations.
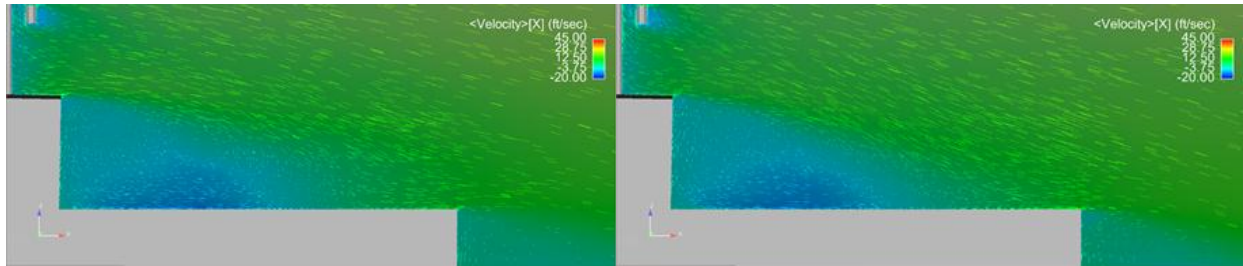

Figure 17: Comparison of CFD simulations for headwind ($\beta = 0°$). Left is grid with 17 million tetrahedral while right is grid with 22 million tetrahedral.

12. A small remotely piloted helicopter, shown in Fig. 18, has been used to identify the turbulent air wake region aft of the YP676 flight deck. As the helicopter, which has a 4.5 ft diameter rotor, is maneuvered through regions in the ship's air wake where there are steep velocity gradients, an IMU mounted on the helicopter records a noticeable change in the helicopter's flight path. Concurrently, the relative position of the helicopter is determined by comparing the GPS derived position of the helicopter with that of a reference position on the ship. Combining these two measurement systems, the locations of sharp gradients in the air wake can be mapped relative to the ship (accurate within one rotor diameter of the helicopter) and compared with CFD simulations of similar wind-over-deck configurations.

When the helicopter encountered the ship air wake there was a noticeable increase in flight path disturbances, as measured by the IMU (Fig. 19), due to interaction with the air wake. These interactions were then manually compared with CFD predictions of the ship air wake with the relative position determined through use of GPS units on both the ship and helicopter. Relative position was determined to be accurate within one meter (approximately 3

ft),[21] which is slightly smaller than the length scale of the main rotor of the helicopter. Figures 20 and 21, respectively, show helicopter detected flight path disturbances superimposed over CFD air wake predictions for both β = 15° and 30°. During underway flight operations the YP's craft master attempted to keep the ship under the same wind over deck condition as based upon the reference anemometer. Since winds typically shift during a given flight the craft master had to adjust ship's course to maintain an approximately constant wind over deck. Shifting winds with subsequent adjustment in ship's course explains the apparent drift of the measured wake towards the port side further aft of the flight deck.

Figures 20 and 21 show good correlation between the location of the YP's air wake from the CFD simulations versus what was measured by the IMU onboard the helicopter during underway testing. However this data analysis method was dependent upon manual review of all data, which is very time consuming and can be subjective.

Figure 18. Radio controlled instrumented helicopter flying astern of YP676 in the Chesapeake Bay.

American Institute of Aeronautics and Astronautics
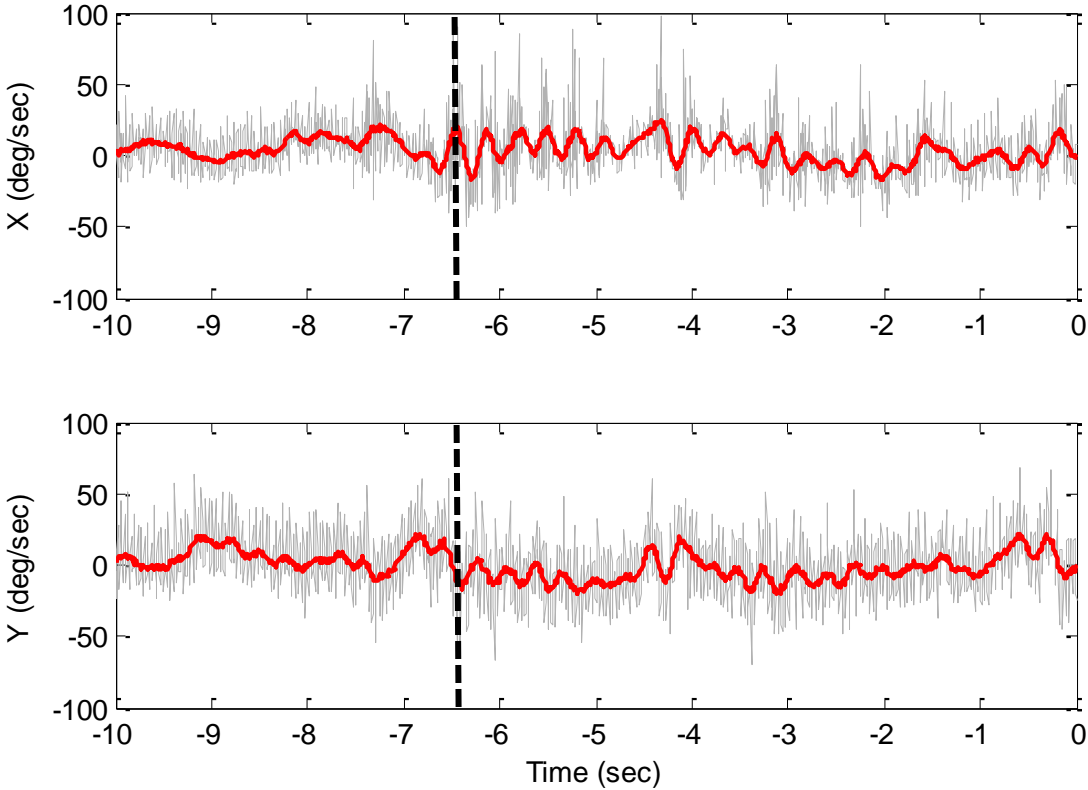
Figure 19. Pitch and roll gyroscopic data along a flight path into the air wake. Dashed line indicates time at which the helicopter entered the wake.
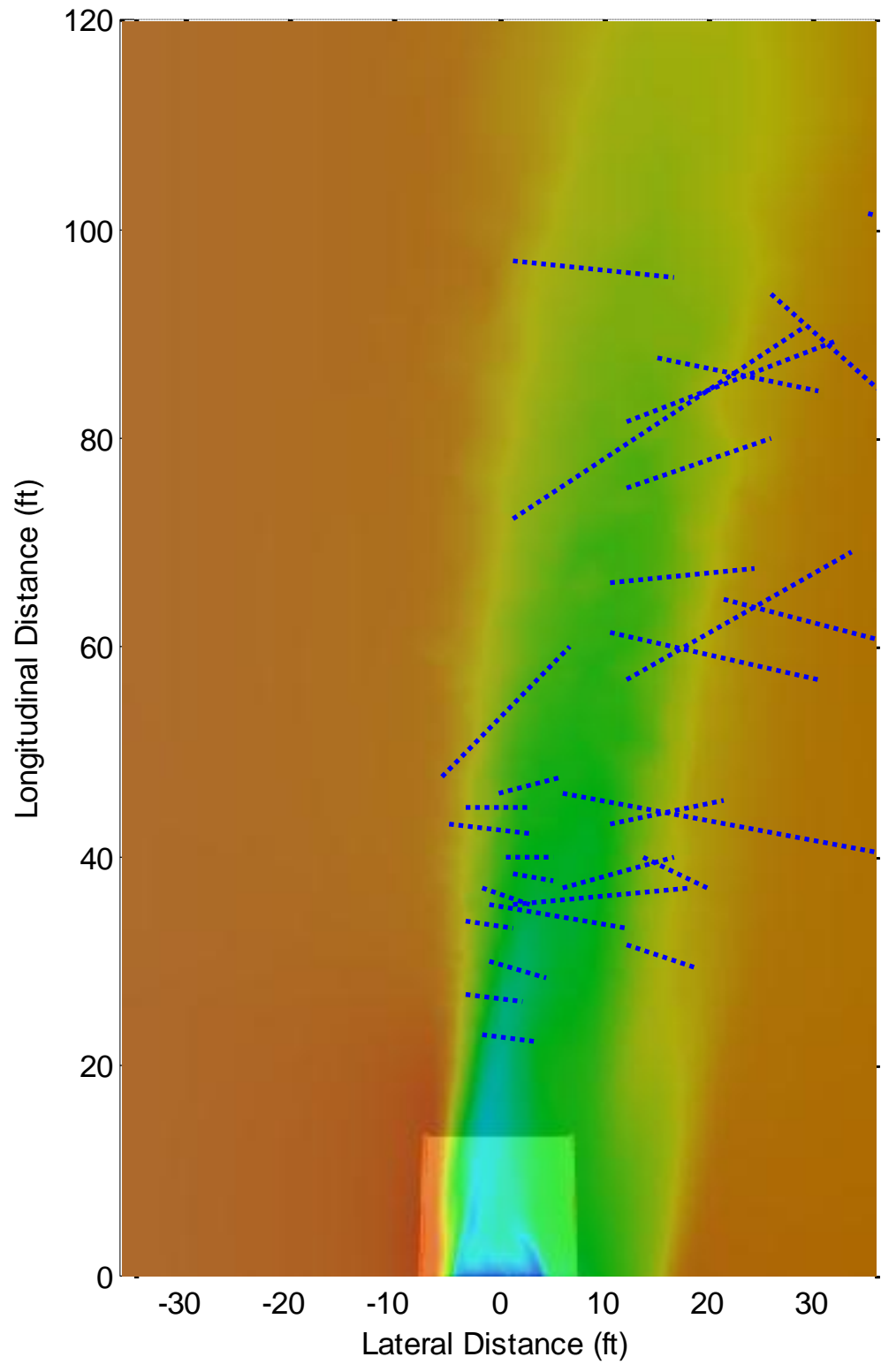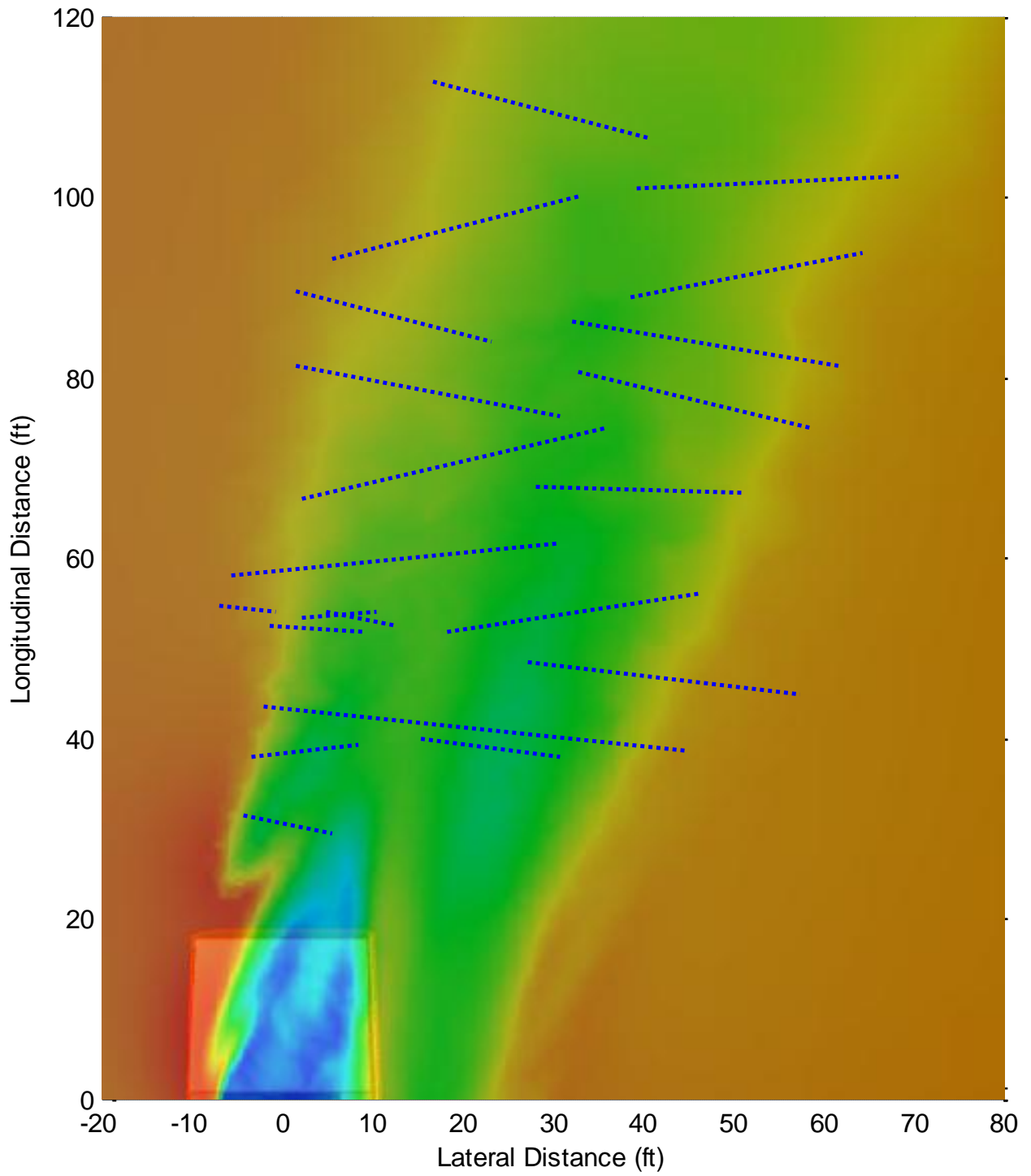
Figure 20. Measured air wake location (blue dashed lines) and CFD simulation (colored background) for β = 15° at the top of the hangar structure.

American Institute of Aeronautics and Astronautics

Figure 21. Measured air wake location (blue dashed lines) and CFD simulation (colored background) for β = 30° at the top of the hangar structure.

American Institute of Aeronautics and Astronautics

IV. Automated Analysis of Off Ship Air Wake Data

In order to reduce the subjective nature of off ship air wake data analysis as discussed above, and to improve analysis efficiency, it is desirable to automate analysis of ship air wake data collected using the instrumented RC helicopter. This section will discuss theoretical development and recent advances in automated data analysis of off ship air wake data.

Since the direction of rotation due to the air wake is generally random and not predictable, it can be inferred that only the magnitude of the IMU vibrations determines the intensity of the air wake. Therefore, when the air wake pattern only is of interest, it is advantageous to use radial component of the gyroscope data rather than the three Cartesian components as it decreases the computational burden during analysis. In the automated system, the gyroscope data is converted to a spherical coordinate system and the absolute magnitude (radial component) is used to automatically detect air wake pulses or peaks. If $\{\omega_x, \omega_y, \omega_z\}$ is the angular velocity of the helicopter in the Cartesian coordinate system, then the radial component of the angular velocity (ω_r) was obtained as:

$$\omega_r = \sqrt{\omega_x{}^2 + \omega_y{}^2 + \omega_z{}^2}.$$

Significant ship air wake causes the helicopter to oscillate vigorously (with large amplitude), which appears as oscillations in the IMU (predominantly in the gyroscope) data. Therefore, whenever the helicopter enters into an air wake zone, an increase in the gyroscope fluctuation readings is expected. This fluctuation will appear as a peak in the gyroscope absolute magnitude (radial) component as well as a peak in the local standard deviation of the gyroscope radial component.

High rotor speed introduces noise in the IMU reading in the form of internal oscillations. Since the frequency of such oscillations is much higher than that caused by the air wake, the effect of the helicopter's own vibrations in the gyroscope output can be nullified by applying a low pass filter. After empirical optimization, a Gaussian low pass filter was applied to the data (with filter window length of 3 sec and Gaussian filter width of 0.5 sec). The resultant waveform is an (absolute) angular velocity of the helicopter caused by the air wake only. If ω_r is the radial component of the raw gyroscope data then filtered the signal (ω_f) is obtained as follows:

$$\omega_f = G(\sigma, L) * \omega_r$$

where * is the mathematical convolution operation and $G(\sigma,L)$ is the Gaussian low pass filter kernel with width σ (number of samples in 0.5 sec of data) and length L (number of samples in 3.0 sec of data).

During an encounter with significant air wake one will observe sudden changes in angular/linear velocities under the effect of large accelerations. To measure the extent of changes in angular velocities, local standard deviation for the gyroscope data (radial component) was calculated by applying a standard deviation filter with a window size of 3 sec. The ith sample of the local standard deviation (ω_s) of the raw gyroscope data radial component (ω_r) is calculated as follows:

$$\omega_s(i) = \sqrt{\frac{\sum_{d=-\frac{L}{2}}^{+\frac{L}{2}} \left(\omega_r(i+d) - \frac{1}{L}\sum_{x=-\frac{L}{2}}^{+\frac{L}{2}} \omega_r(i+x) \right)^2}{L}} \; ; i \in I \,[1,N]$$

where N is total number of samples in ω_r.

Since a simultaneous rise is expected in the filtered gyroscope data and its standard deviation data, the two waveforms were multiplied (point-to-point multiplication) to analyze air wake conditions. For convenience, we are referring to this generated waveform as air wake data (A_ω) in the rest of the paper.

$$A_\omega(i) = \omega_s(i) \times \omega_f(i); \; i \in I \,[1,N]$$

Figure 22 shows the data related to various steps of IMU data processing. In the upper plot, the green colored data is the magnitude of the raw gyroscope data in spherical coordinates, which is very noisy due to the presence of the helicopter's vibrations. The blue colored waveform is the low pass filtered output of the raw gyroscope data and the red colored waveform shows the local standard deviation of the raw gyroscope data. The lower plot shows air wake data resulting from the product of the low pass filtered data and local standard deviation of the gyroscope output.
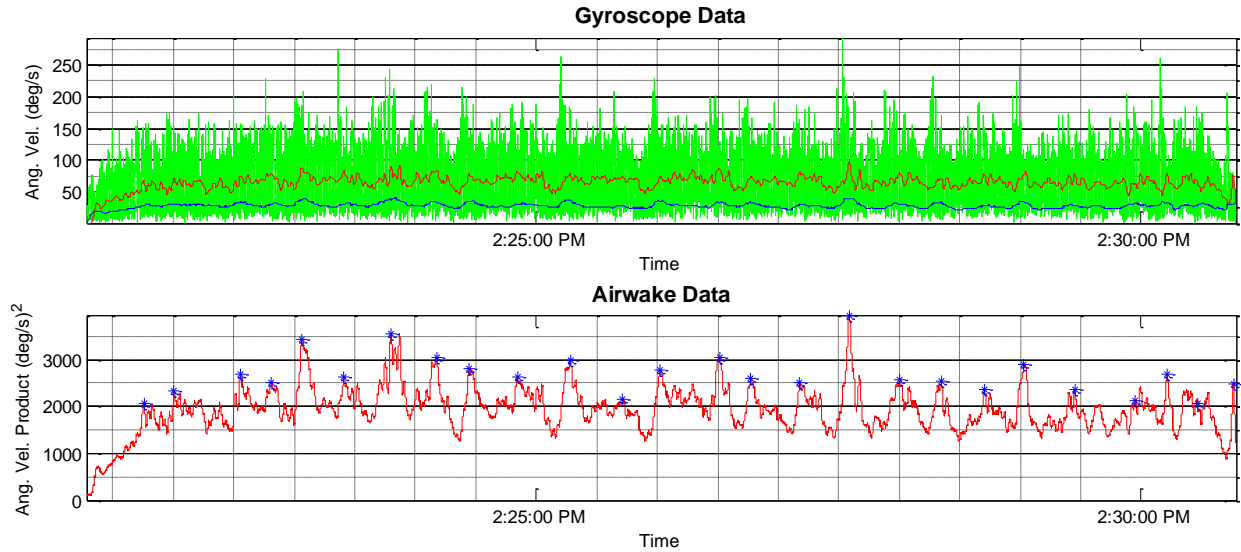
Figure 22: Sample processing of IMU data. Upper figure is raw data (green) plus low pass filtered data (blue) and local standard deviation (red). Lower figure shows processed data.

To determine the spatial distribution of air wake around the ship deck, the helicopter relative position and the IMU data were fused into a single plot. Since the IMU and the GPS data were acquired at different sampling rates (at 128 Hz and 10 Hz, respectively), the GPS data was interpolated to resample it to the IMU acquisition rate.

Since for detection of air wake we should have simultaneous peaks in both absolute angular velocity and standard deviation of the absolute angular velocity, A_ω was used to detect local maxima/peaks. The local maxima peak points that were retained were only those which were at least 15 sec apart and were at least 1.5 times higher than the standard deviation (of the whole waveform data) of the points in the neighborhood of the 10 sec window. The value of the neighborhood window size and the adaptive threshold are experimentally determined such that these values work well for a wide range of flight experiments. The location of the peaks can be related to the air wake interactions. The peaks in air wake data A_ω were also compared with air wake peaks detected by visual inspection of the helicopter flight video recordings. There was a good correlation in the occurrence of peaks detected by the two methods. Figure 23 shows air wake data A_ω plotted on the GPS trajectory as a color plot with the red color indicating high air wake intensity. Figure 24 shows the CFD predicted air wake for a headwind ($\beta = 0°$) condition. Comparing Figs. 23 and 24, regions of detected maximum air wake intensity correspond well to locations predicted by CFD.

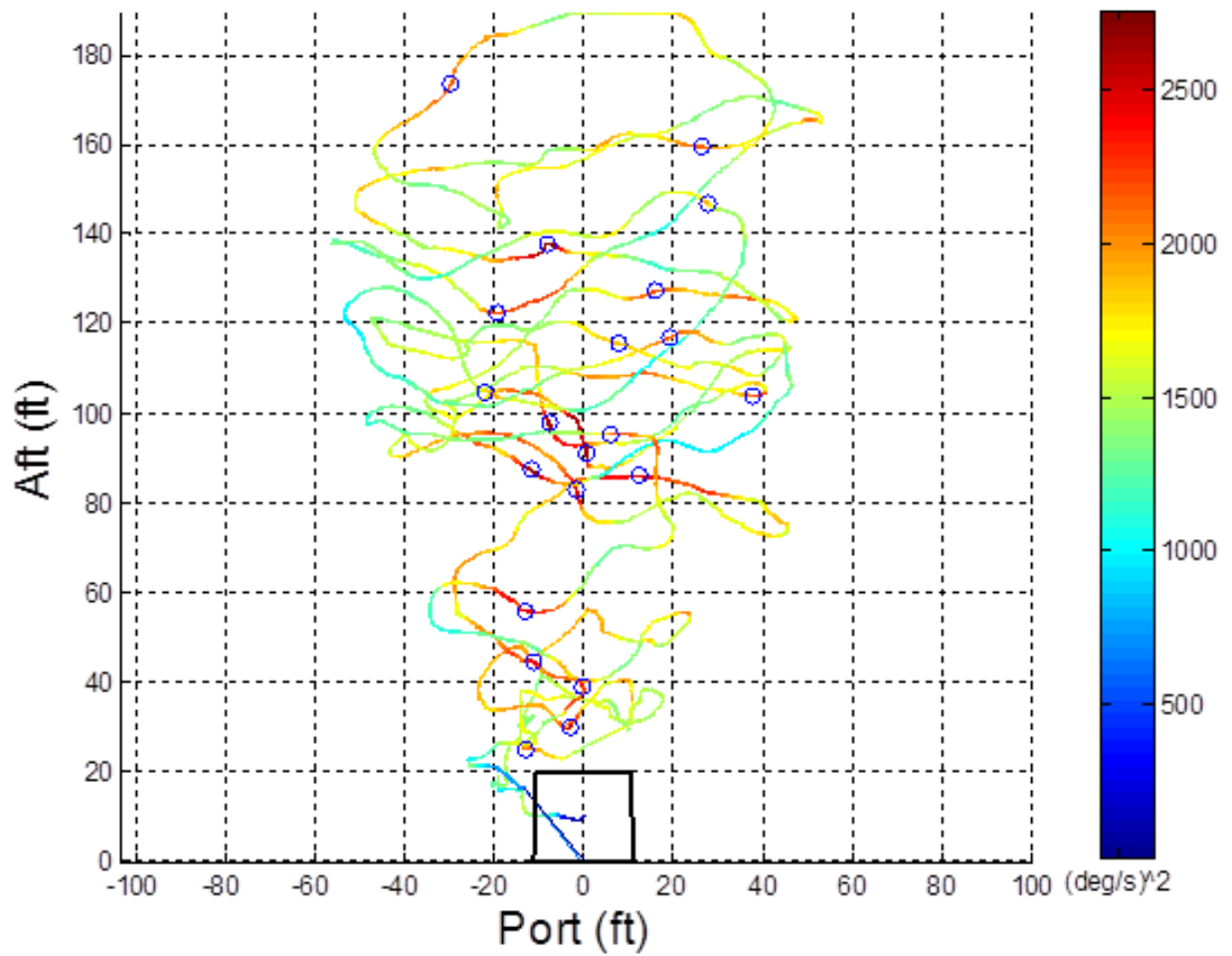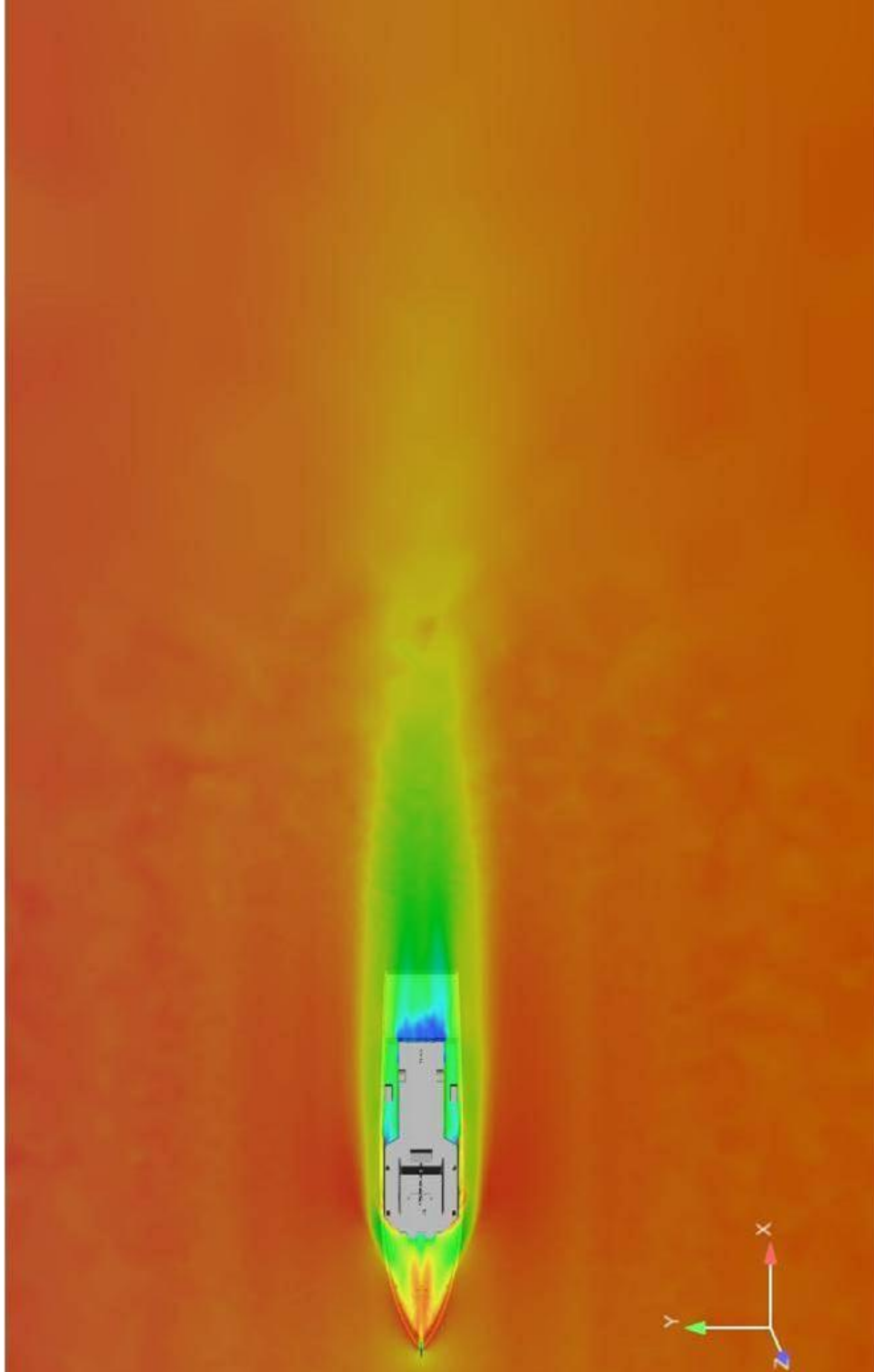**Figure 23. β = 0° air wake data A_ω plotted vs. helicopter relative position. Red color indicates high air wake intensity.**

Figure 24. 20 knot, with atmospheric boundary layer, β = 0° CFD predicted air wake data. Regions that are yellow or green represent regions of decelerated flow and maximum air wake.

To estimate the direction of the air wake flow, accelerometer data was used rather than gyroscope data because the direction of acceleration caused by air wake is the same as the air wake flow. Since the accelerometer data from the IMU also contains component of acceleration due to gravity, the direction of the accelerometer data vector is not in the same direction of the air wake flow. Hence the raw accelerometer data could not be used for determining air wake direction. To solve this problem, the absolute orientation of the IMU (helicopter) in the global frame of reference (obtained from the IMU) was used. From this orientation, the contribution of gravity into each of the Cartesian components of the accelerometer data was calculated. Then the Cartesian components of the gravity vector in the IMU's frame of reference were subtracted from the accelerometer data to estimate net 'non-gravitational' acceleration on the helicopter. The direction angles (longitudinal and latitudinal) for the accelerations where also calculated in spherical coordinate system. This procedure provides a good estimation of the air wake direction using the accelerometer data in the helicopter's frame of reference. If $\{a_x, a_y, a_z\}_h$ is the acceleration data obtained from the IMU in the helicopter's frame of reference and $\{0,0,g\}_g$ is the acceleration due to gravity in the global coordinate system, the non-gravitational component of the acceleration (A_a) on the helicopter in its frame of reference is given by:

$$A_a = \begin{bmatrix} a_x \\ a_y \\ a_z \end{bmatrix} - \begin{bmatrix} R_{\alpha\beta\gamma} \end{bmatrix} \begin{bmatrix} 0 \\ 0 \\ g \end{bmatrix}_g \; ;$$

$$\begin{bmatrix} R_{\alpha\beta\gamma} \end{bmatrix} = \begin{bmatrix} \cos\beta\cos\gamma & -\cos\alpha\sin\gamma + \sin\alpha\sin\beta\cos\gamma & \sin\alpha\sin\gamma + \cos\alpha\sin\beta\cos\gamma \\ \cos\beta\sin\gamma & \cos\alpha\cos\gamma + \sin\alpha\sin\beta\sin\gamma & -\sin\alpha\cos\gamma + \cos\alpha\sin\beta\sin\gamma \\ -\sin\beta & \sin\alpha\cos\beta & \cos\alpha\cos\beta \end{bmatrix}$$

where $\begin{bmatrix} R_{\alpha\beta\gamma} \end{bmatrix}$ is a 3×3 rotation matrix representing the orientation of the helicopter in the global coordinate system through Euler angles α, β and γ about *x, y* and *z* axes, respectively. Since the orientation of the helicopter with respect to the boat is kept relatively constant, the direction of air wake in the helicopter's frame of reference is the same as in the boat's frame of reference. Figure 25 shows instantaneous magnitude and direction of the air wake plotted on the helicopter's trajectory. This method shows air wake direction as primarily downward though anecdotal evidence would suggest that there should be a more even distribution of air wake direction both upward and downward. Resolution of this issue requires further analysis.
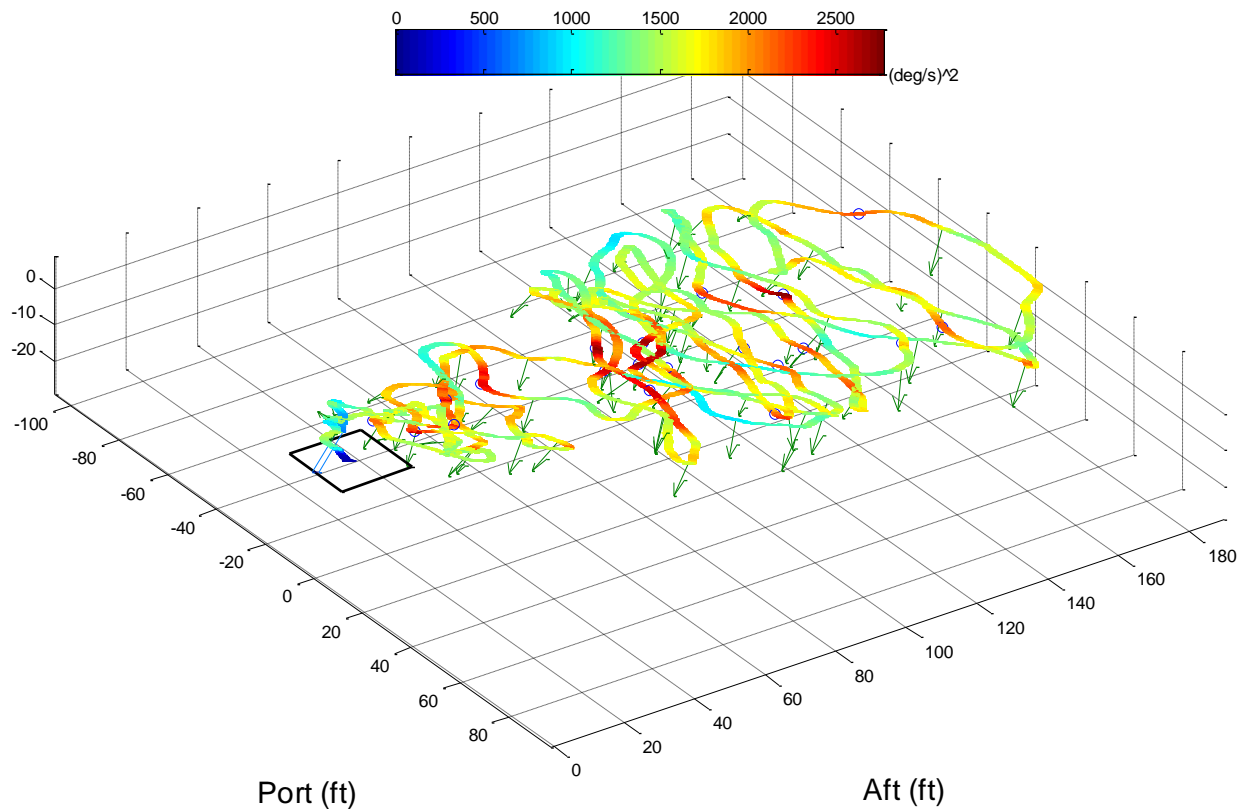
Figure 25. Instantaneous magnitude of A_ω (color) and direction of air wake (arrows) superimposed over helicopter trajectory.

V. Conclusions and Future Work

The present work has shown the usefulness of an automated method for the analysis of ship air wake data collected using an instrumented RC helicopter. Regions of significant air wake detected by the automated analysis method correspond to regions predicted by high resolution CFD simulations.

Additional effort will be required to develop validated CFD and other investigative tools that would be useful in determination of rotary wing launch and recovery envelopes. Specific areas which we will investigate in the future include:

1. The IMU carried by the RC helicopter also detects vibrations induced due to pilot control inputs. These pilot induced IMU vibrations may be misinterpreted as arising due to air wake interactions. We are currently developing a method to remove pilot induced vibrations from air wake data collected during flight operations. This method will involve subtracting out known IMU responses to specific flight control inputs that were measured in benign or no wind conditions.

2. Collect additional *in situ* data above the flight deck for more off-axis wind conditions, specifically $\beta = 45°$ and $90°$ data. Comparisons will also be made between *in situ* data and CFD simulations for $\beta = 45°$ and $90°$. Wind tunnel data for $\beta > 30°$ are not obtainable due to blockage effects.

3. Collect *in situ* data for the immediate region around but outside the flight deck. Data in regions within 5-6 feet of the flight deck will be collected through the use of boom mounted anemometers. Alternative sampling techniques such as laser-based instruments will also be investigated.

4. Collect extensive atmospheric boundary layer data to quantify the average boundary layer velocity profile encountered during underway testing. This average boundary layer will then be modeled in updated CFD simulations and in wind tunnel testing to see if a closer match can be obtained in flow velocity magnitude.

American Institute of Aeronautics and Astronautics

5. A wind tunnel Reynolds number sensitivity study will be performed to determine if ship air wake correlations developed using matched Reynolds numbers between *in situ* and wind tunnel testing can be extended to cases where it is not possible to match Reynolds numbers in wind tunnel testing (e.g. wind tunnel testing of a 1% or smaller ship model).

6. Investigate passive modification of ship air wakes previously studied by Shafter.[25] During the summer of 2012 YP676 was modified with the addition of flow control fences as shown in Fig. 26. Underway *in situ* and wind tunnel data for the modified vessel is being collected and compared with CFD simulations, performed with flow control fences and a model atmospheric boundary layer, to see if ship air wake changes can be predicted computationally and whether flow control fences or similar designs could reduce the severity of ship air wake impact on rotary wing aircraft.

Figure 26. Flow control fences (blue wedges) added to the top, port and starboard sides of hangar structure and starboard side of flight deck.

Acknowledgments

References

[1]"Helicopter operating procedures for air-capable ships NATOPS manual," NAVAIR 00-08T-122, 2003.

[2]Guillot, M.J. and Walker, M.A., "Unsteady analysis of the air wake over the LPD-16," *AIAA 2000-4125: 18th Applied Aerodynamics Conference*, Denver, Colorado, 2000.

[3]Guillot, M.J., "Computational simulation of the air wake over a naval transport vessel," *AIAA Journal*, Vol. 40, No. 10, 2002, pp. 2130-2133.

[4]Lee, D., Horn, J.F., Sezer-Uzol, N., and Long, L.N, "Simulation of pilot control activity during helicopter shipboard operations," *AIAA 2003-5306: Atmospheric Flight Mechanics Conference and Exhibit*, Austin, Texas, 2003.

[5]Carico, D., "Rotorcraft shipboard flight test analytic options," *Proceedings 2004 Institute of Electrical and Electronics Engineers (IEEE) Aerospace Conference*, Vol. 5, Big Sky, Montana, 2004.

[6]Lee, D., Sezer-Uzol, N., Horn, J.F., and Long, L.N., "Simulation of helicopter ship-board launch and recovery with time-accurate air wakes," *Journal of Aircraft*, Vol. 42, No. 2, 2005, pp. 448-461.

[7]Geder, J., Ramamurti, R. and Sandberg, W.C., "Ship air wake correlation analysis for the San Antonio Class Transport dock Vessel," Naval Research Laboratory paper MRL/MR/6410-09-9127, May 2008.

[8]Polsky, S., Imber, R., Czerwiec, R., & Ghee, T., "A Computational and Experimental Determination of the Air Flow Around the Landing Deck of a US Navy Destroyer (DDG): Part II," *AIAA-2007-4484: 37th AIAA Fluid Dynamics Conference and Exhibit*, Miami, Florida, 2007.

[9]Roper, D. M., Owen, I., Padfield, G.D. and Hodje, S.J., "Integrating CFD and pilot simulations to quantify ship-helicopter operating limits," *Aeronautical Journal*, Vol. 110, No. 1109, 2006, pp. 419-428.

[10]Strang, W.Z., Tomaro, R.F., and Grismer, M.J., "The Defining Methods of Cobalt60: A Parallel, Implicit, Unstructured Euler/Navier-Stokes Flow Solver," *AIAA-99-0786: 37th Aerospace Sciences Meeting and Exhibit*, Reno, Nevada, January 1999.

[11]Boris, J., Grinstein, F., Oran, E., Kolbe, R., "New Insights into Large Eddy Simulation," *Fluid Dynamics Research*, Vol. 10, 1992, pp.199-228.

[12]Polsky, S.A., "A Computational Study of Unsteady Ship Air wake," *AIAA 2002-1022: 40th AIAA Aerospace Sciences Meeting and Exhibit*, Reno, Nevada, 2002.

[13]Snyder, M.R., et al., "Determination of Shipborne Helicopter Launch and Recovery Limitations Using Computational Fluid Dynamics," *American Helicopter Society 66th Annual Forum*, Phoenix, Arizona, 2010.

[14]Snyder, M.R., et al., "Comparison of Experimental and Computational Ship Air Wakes for YP Class Patrol Craft," *American Society of Naval Engineers Launch and Recovery Symposium*, Arlington, VA, December 2010.

[15]Snyder, M.R., Kang, H.S., Brownell, C.J., Luznik, L., Miklosovic, D.S., Burks, J.S. and Wilkinson, C.H., "USNA Ship Air Wake Program Overview," *AIAA 2011-3153: 29th AIAA Applied Aerodynamics Conference, Honolulu*, Hawaii, June 2011.

[16]Roberson, F.D., Kang, H.S. and Snyder, M.R., "Ship air wake CFD comparisons to wind tunnel and YP boat results," *AIAA 2011-3156: 29th AIAA Applied Aerodynamics Conference*, Honolulu, Hawaii, June 2011.

[17]Miklosovic, D.S., Kang, H.S. and Snyder, M.R., "Ship Air Wake Wind Tunnel Test Results," *AIAA 2011-3155: 29th AIAA Applied Aerodynamics Conference*, Honolulu, Hawaii, June 2011.

[18]Snyder, M.R. and Kang, H.S., "Comparison of Experimental, Wind Tunnel and Computational Ship Air Wakes for YP Class Patrol Craft," *AIAC-2011-058: 6th Anakara International Aerospace Conference*, Ankara, Turkey, September 2011.

[19]Snyder, M.R. and Kang, H.S., "Comparison of Experimental and Computational Ship Air Wakes for YP Class Patrol Craft," *AIAA 2011-7045: Centennial of Naval Aviation Forum*, Virginia Beach, Virginia, September 2011.

[20]Metzger, J.D., Snyder, M.R., Burks, J.S. and Kang, H.S., "Measurement of Ship Air Wake Impact on a Remotely Piloted Aerial Vehicle," *American Helicopter Society 68th Annual Forum*, Fort Worth, Texas, May 2012.

[21]Metzger, J.D., "Measurement of Ship Air Wake Impact on a Remotely Piloted Aerial Vehicle," United States Naval Academy Trident Scholar Project report no. 406, May 2012.

[22]Snyder, M.R., Kang, H.S. and Burks, J.S., "Comparison of Experimental and Computational Ship Air Wakes for a Naval Research Vessel," *AIAA 2012-2897: 30th Applied Aerodynamics Conference*, New Orleans, Louisiana, June 2012.

[23]Snyder, M.R., Kang, H.S., Brownell, C.J. and Burks, J.S., "Validation of Ship Air Wake Simulations and Investigation of Ship Air Wake Impact on Rotary Wing Aircraft," *American Society of Naval Engineers Launch and Recovery Symposium*, Linthicum, MD, November 2012.

[24]Snyder, M.R., Kang, H.S., Brownell, C.J. and Burks, J.S., "Validation of Ship Air Wake Simulations and Investigation of Ship Air Wake Impact on Rotary Wing Aircraft," *Naval Engineers Journal*, 2013, in press.

[25]Shafter, D.M., "Active and Passive Flow Control over the Flight Deck of Small Naval Vessels," Master of Science Thesis, Aerospace Engineering Department, Virginia Polytechnic Institute and State University, Blacksburg, Virginia, April 2005.